ELSEVIER

Nuclear Instruments and Methods in Physics Research A 491 (2002) 54–68

NUCLEAR INSTRUMENTS & METHODS IN PHYSICS RESEARCH Section A

www.elsevier.com/locate/nima

A detailed Monte Carlo simulation for the Belle TOF system

J.W. Nam[a,*], Y.I. Choi[a], D.W. Kim[a], J.H. Kim[a], B.C.K. Casey[b], M. Jones[b], S.L. Olsen[b], M. Peters[b], J.L. Rodriguez[b], G. Varner[b], Y. Zheng[b], N. Gabyshev[c], H. Kichimi[c], J. Yashima[c], J. Zhang[d], T.H. Kim[e], Y.J. Kwon[e]

[a] *Department of Physics, Sungkyunkwan University, Chungchundong, 300, Suwonm, South Korea*
[b] *University of Hawaii, Honolulu HI, USA*
[c] *High Energy Accelerator Research Organization (KEK), Tsukuba, Japan*
[d] *University of Tsukuba, Tsukuba, Japan*
[e] *Yonsei University, Seoul South Korea*

Received 30 April 2002; accepted 4 June 2002

Abstract

We have developed a detailed Monte Carlo simulation program for the Belle time-of-flight (TOF) system. Based on GEANT simulation, it takes account of all physics processes in the TOF scintillation counters and readout electronics. The simulation reproduces very well the performance of the Belle TOF system, including the dE/dx response, the time walk effect, the time resolution, and the hit efficiency due to beam background. In this report, we will describe the Belle TOF simulation program in detail.

PACS: 07.05.Tp; 29.40.Mc

Keywords: Detector simulation; Time-of-flight

1. Introduction

A time-of-flight (TOF) detector [1,2] system using plastic scintillation counters is very powerful for particle identification (PID) in e^+e^- collider detectors [2,3]. A TOF system with 100 ps time resolution is effective for particle momenta below about 1.2 GeV/c, which encompasses 90% of the particles produced in $\Upsilon(4S)$ decays. It can provide clean and efficient flavor tagging for CP violation studies in B meson decays in a B-factory experiment.

A reliable Monte Carlo (MC) simulator is a good tool to understand the detector system and is important for minimizing experimental systematic uncertainties for physics analysis. Although one simple simulation method is a parametrization based on real data, it does not provide precise simulation for complex experimental situations, such as multi-track hits, hadronic interactions in the TOF counter, and shower leakage from the calorimeter outside the TOF system.

We have developed a full detector simulator for the TOF system. Based on GEANT3 [4], it

*Corresponding author.
E-mail address: jwnam@bmail.kek.jp (J.W. Nam).

0168-9002/02/$ - see front matter
PII: S0168-9002(02)01231-7

includes the simulation of all physics processes involving scintillation light production and its propagation in the TOF counters, the production of signal pulses in the photomultiplier tubes (PMT), the electronics process in the discriminator and the charge to time converter (QTC), and the effects of beam background.

In this report, we describe the Belle TOF detector simulation. In Section 2, we briefly introduce the Belle TOF system. In Section 3 we describe the simulation model and the main algorithm for each process. Finally, we compare the simulation results with experimental data in Section 4. Section 5 contains conclusions.

2. TOF system in the Belle detector

The Belle detector is a large solid-angle spectrometer based on a 1.5 T superconducting solenoid magnet; a detailed description can be found elsewhere [2]. Fig. 1 shows the Belle detector.

The TOF system consists of 64 TOF/TSC modules located at a radius of 1.2 m from the interaction point, which cover a polar angle of 33.7–120.8°. The design of one TOF module is shown in Fig. 2. A module consists of two TOF counters of 4 cm thickness, viewed at both ends by PMTs, and one 0.5 cm thick TSC counter, viewed only at the backward (i.e. large angle) end.

In order to get sufficient gain in a 1.5 T field, a fine mesh-photomultiplier (FM-PMT) [5] is used. This tube has 24 fine mesh dynodes of 2000 mesh/in., and its size is 8 cm in length and 5.08 cm in diameter. Its bialkali photocathode covers 50% of the end area of each TOF counter. The PMT gain is adjusted to be about 1×10^6, which requires a high voltage of about 2100 V in the 1.5 T field. The FM-PMTs are attached to the TOF counter ends with an air gap of ~ 0.1 mm that selectively passes early arrival photons and reduces the PMT anode current. For the TSC counters, the tubes are glued to light guides that are attached to the scintillator. Table 1 lists the characteristic parameters of the TOF scintillator and the FM-PMT used in this simulation.

Fig. 3 shows a block diagram of the TOF front end electronics (TOFFEE). Each PMT signal is split into two. One-half is sent to a QTC for charge measurement. The other half goes to generate two output signals by application of different threshold levels. The high level (HL) signal is used to provide

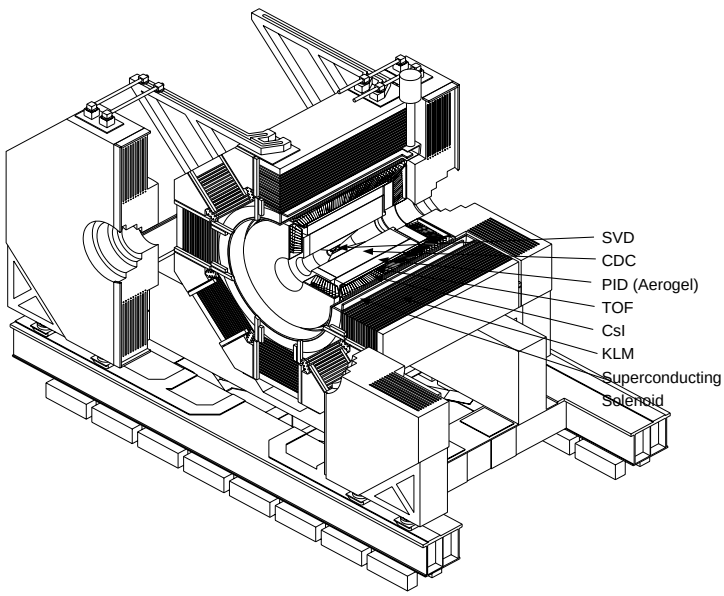

Fig. 1. Cut-away view of the Belle detector.

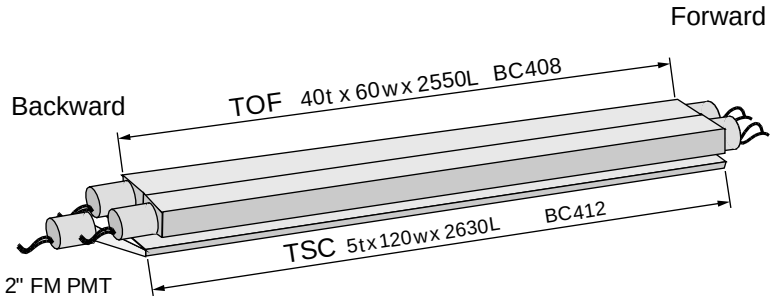

Fig. 2. TOF/TSC module.

Table 1
Characteristic parameters of the TOF scintillator and the FM-PMT

TOF scintillator (BC408)	
Base	Polyvinyltoluene
Density	1.032
Refractive index	1.58
Rise time	0.9 ns
Decay time	2.1 ns
Pulse width	~2.5 ns
Light attenuation length	~300 cm
Wavelength of maximum emission	425 nm
FM PMT (R6680)	
Effective photocathode diameter	39 mm
Transit time spread	320 ps (r.m.s)
Quantum efficiency	~0.21
Electron collection factor	0.6
Rise time	3.5 ns
Fall time	4.5 ns
Pulse width	6 ns (FWHM)

a gate to the QTC, and the low level (LL) signal is fed to a time stretcher (TS) for time measurement.

3. Simulation procedure

Fig. 4 shows the outline of the Belle TOF simulation program. It consists of the GEANT part, the main TOF simulation part including the scintillator, the PMT and discriminator processes, and the beam background merge.

GEANT provides the hit information for a particle passing through the scintillator, including the four vector, hit position, time, and energy loss.

Using the hit information from GEANT, scintillation light is produced. The light is then propagated in the TOF scintillator until it arrives at a PMT and makes a signal pulse. Finally, a pulse larger than the HL threshold makes a gate to measure the charge and timing of the signal. The main detector characteristics, such as the time resolution, are simulated in this part.

In order to take into account the effect of beam background, real data taken with random triggers, which represent the beam background, are merged into the MC output. The inefficiency due to the dead time of the QTC is simulated here.

3.1. Geant simulation up to the TOF counters

The geometrical and material configuration of the Belle detector is implemented in the Belle GEANT full simulator [2]. Not only all sub-detector components, but also materials for the support, cooling structures, and readout cables are included. These allow realistic simulation of a primary particle that goes through the inner sub-detector (and materials) up to the TOF scintillator and of secondary particles that are produced in the inner and outer materials.

The material of the TOF/TSC scintillator is defined as a mixture of hydrogen and carbon. The atomic ratio is assumed to be 1:1. The density of this material is 1.032.

The GEANT hit information for a particle traversing the scintillator volume is recorded at discrete steps along the particle trajectory. For a particle with a given energy, the step size is automatically calculated by GEANT depending

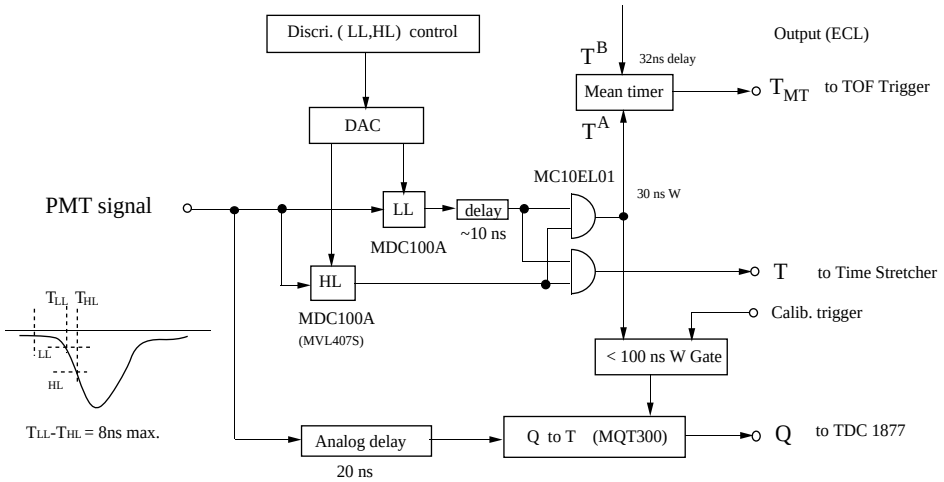

Fig. 3. Block diagram of the TOF front end electronics (TOFFEE).

on particle species and on the characteristics of the current medium [4]. Fig. 5 shows the time at the first step and energy loss distributions for 2.0 GeV/c μ^- which enter perpendicular to the TOF counter.

3.2. Scintillation process

Using the step information from GEANT, we reconstruct a continuous path connecting each step in the scintillator volume. Scintillation light is uniformly emitted along this path. The time t_{traj} on this path for each light emission event is calculated by using the four vectors of the particle.

The number of photons is proportional to the energy loss of the particle, at a rate assumed to be one photon per 100 eV [6]. The angular distribution of the emitted light is isotropic. The time profile of scintillation emission is simulated by using the emission time (t_{emit}) probability function [7],

$$E(t_{\mathrm{emit}}) = \frac{1}{1+R}\left(\frac{\mathrm{e}^{-t_{\mathrm{emit}}/\tau_2} - \mathrm{e}^{-t_{\mathrm{emit}}/\tau_1}}{\tau_2 - \tau_1} + \frac{R}{\tau_3}\mathrm{e}^{-t_{\mathrm{emit}}/\tau_3}\right) \quad (1)$$

where τ_1 and τ_2 are two fast decay time constants, τ_3 is the decay time of the slow component, and R is the ratio of the slow to fast components. Since the signal timing is determined at the leading edge in the discriminator, τ_1 and τ_2 are the most important parameters for TOF simulation. We use $\tau_1 = 0.9$ ns and $\tau_2 = 2.1$ ns; these values are chosen so that this function has the same rise time as the BC408 scintillator light output. The values $\tau_3 = 14.2$ ns and $R = 0.27$ are given in Ref. [7]. Fig. 6 shows the $E(t_{\mathrm{emit}})$ distribution.

3.3. Light propagation

The scintillation light is propagated by total internal reflection and arrives at the PMTs located at the ends of the scintillator. We assume that light which has an emission angle within the trapping angle (θ_{trap}) can traverse the air gap to reach the PMT, while the remaining light escapes from the scintillator volume without total reflection or is lost during the endless total reflection between the two ends of the TOF scintillator (see Fig. 7(1)). The angle θ_{trap} is given by

$$\theta_{\mathrm{trap}} = \sin^{-1}\left(\frac{n_{\mathrm{air}}}{n_{\mathrm{scint}}}\right) \quad (2)$$

where n_{air} and n_{scint} are the refractive indices of the air and scintillator, respectively.

By assuming perfect internal reflection on each of the four surfaces of the TOF counter, the light propagation length in the counter is calculated (see

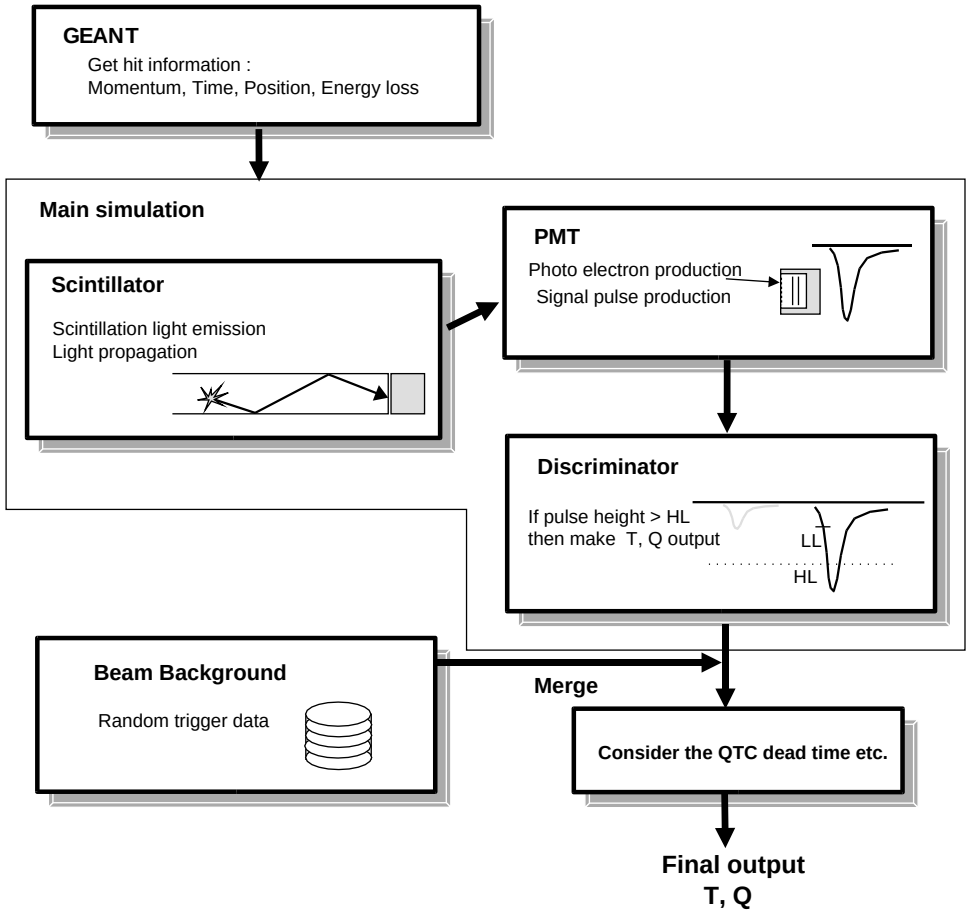

Fig. 4. Block diagram of the simulation program.

Fig. 7(2)) as

$$l_{\mathrm{pro}} = \frac{d}{\cos\theta} \tag{3}$$

where d is the distance from the light emission position to the end surface of the scintillator and θ is the polar angle of the emitted light. This technique effectively reduces the CPU time, while the result is equivalent to a full simulation of light propagation. Fig. 8 shows the path length distribution of light which is produced at $z = 0$ and reaches the forward PMT.

The light propagation time in the scintillator is obtained by

$$t_{\mathrm{pro}} = \frac{l_{\mathrm{pro}}}{v_{\mathrm{scint}}} \tag{4}$$

where $v_{\mathrm{scint}} = c/n_{\mathrm{scint}}$ is the velocity of light in the scintillator.

Attenuation in the TOF counter is simulated according to

$$R(l_{\mathrm{pro}}) = \mathrm{e}^{-l_{\mathrm{pro}}/\lambda_{\mathrm{pro}}} \tag{5}$$

where λ_{pro} is the attenuation length in the scintillator material. We use $\lambda_{\mathrm{pro}} = 400$ cm, which is measured with real data.

The mismatch of the rectangular cross-section of the TOF counter to the round PMT results in light loss (see Fig. 7(3)). In the simulation, the number of photons is reduced by the ratio of the TOF end area to the effective area of the PMT photocathode.

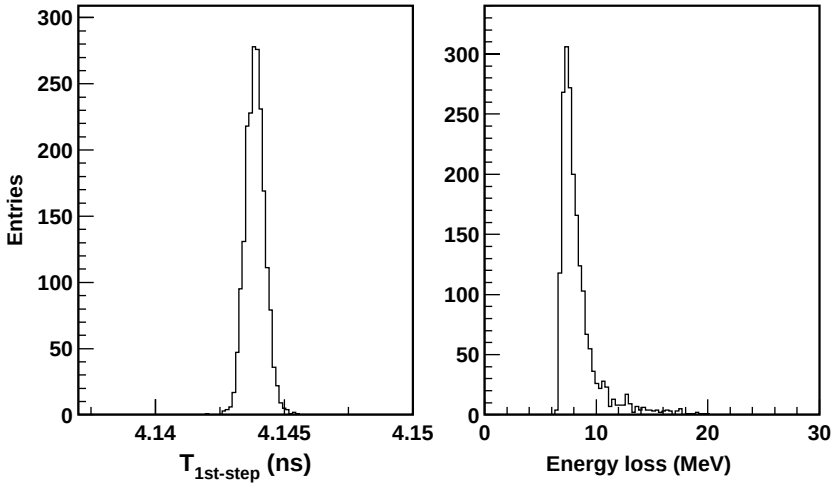

Fig. 5. First-step time (left panel) and energy loss (right panel) distributions.

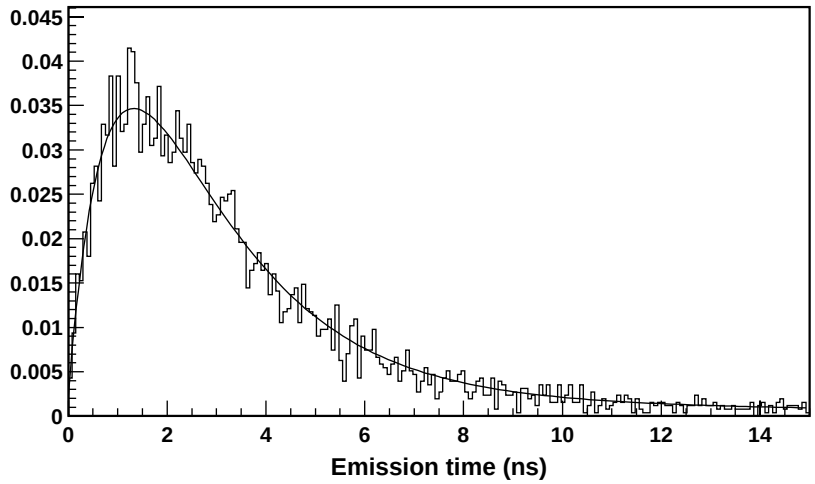

Fig. 6. Emission time probability for scintillation light. The line is the function, the histogram is the simulated result.

3.4. PMT response

We consider the angular response (R_{angle}) of PMT sensitivity, which is a dependence on the angle of incident light on the photocathode [8],

$$R_{\text{angle}} = \cos\theta_i \tag{6}$$

where θ_i is the light incident angle at the PMT front glass. We find 0.66 for the efficiency averaged over all arrival directions at the PMT. The number of photons is reduced by this factor.

At the PMT photocathode, photoelectrons are produced with a probability which is called the quantum efficiency. The average quantum efficiency of the photocathode is calculated to be 0.21 for the spectrum from the BC408 scintillator. Also, the number of photoelectrons is reduced by a factor of 0.6, called the collection factor, due to the fine mesh dynode structure. We reduce the number of generated photoelectrons by these factors.

The transit time of a single photoelectron signal in a FM-PMT, t_{TT}, is modeled by a transit time

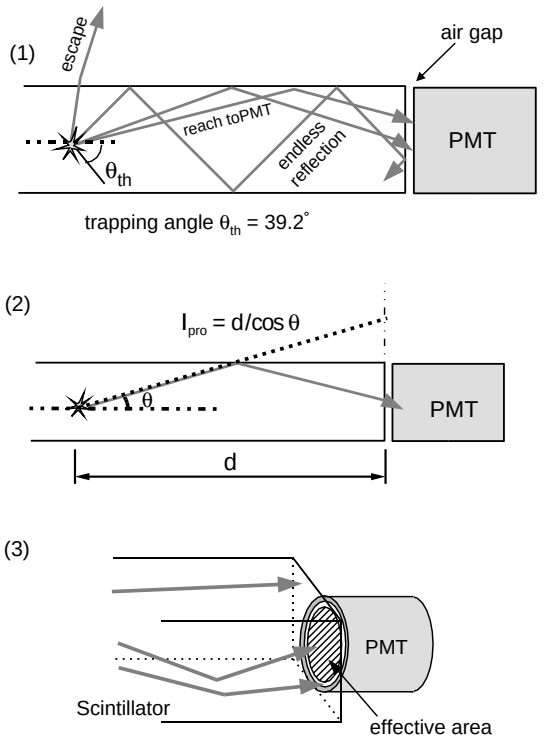

Fig. 7. Light propagation in a scintillator counter.

(TT) of 5.5 ns and a r.m.s. transit time spread (TTS) of 0.31 ns, which are measured for the R6680 FM-PMT. By adding the smeared transit time to the photon timing information described in the previous section, the pivot time of single photoelectron signal at the anode is obtained,

$$t_{\mathrm{pe}} = t_{\mathrm{traj}} + t_{\mathrm{emit}} + t_{\mathrm{pro}} + t_{\mathrm{TT}}. \tag{7}$$

Fig. 9(1) shows the time distribution of the photoelectrons at the anode for a typical event, a 2.0 GeV/c μ^- incident on a TOF counter at $z = 0$.

To simulate the time walk effect due to the leading edge discrimination scheme used for the Belle TOF, a time response function $v_i(t)$ for a single photoelectron is introduced. Using this response function, the PMT output signal is obtained by summing all the single photoelectron signals in the PMT for an event,

$$V_{\mathrm{PMT}}(t) = \sum_{i=1}^{n_{\mathrm{pe}}} v_i(t) \tag{8}$$

where

$$v_i(t) = GC_{\mathrm{e}} \frac{t^2 \mathrm{e}^{-t^2/\tau^2}}{\int t^2 \mathrm{e}^{-t^2/\tau^2}\,\mathrm{d}t}. \tag{9}$$

Here G is the gain of PMT, C_e is the conversion factor for charge to voltage, and τ is the time constant. We use $\tau = 6$ ns so that the rise time of this function is the same as that of an R6680 PMT, and 25 ps time bin size which is the same as the least count of the Belle TOF readout system [1].

Fig. 9(2) shows a typical PMT output signal for the same event as shown in Fig. 9(1). The simulated signal is consistent with actual signals observed in the Belle TOF counters in both pulse height and rise time.

3.5. Simulation of readout electronics

Each PMT signal is examined by readout electronics using double thresholds. A signal larger than the HL threshold provides a gate to measure the signal timing (TDC) which is given at the moment when the PMT pulse crosses the LL threshold in the discriminator simulation. We use the same LL threshold as the real experiment (50 mV). A HL value 50% higher than that in the real experiment (150 mV) is used for fine tuning of the hit inefficiency, which is caused by PMT-to-PMT gain variation in the real experiment.

Finally, we introduce a timing uncertainty, parametrized by a Gaussian with a width of 45 ps, which is due to the uncertainty of the beam crossing time ($t = 0$) determination, the time jitter caused by electronic noise in the discriminators, and the time jitter in the TS readout. Fig. 10(1) shows the TDC distribution for perpendicular incidence on a TOF counter, and Fig. 10(2) shows TDC values as a function of particle hit position (z-hit) along the counter. The z-hit value is obtained by extrapolating the particle's trajectory using tracking information from the central drift chamber (CDC) [2]. The filled circles in Fig. 10 are data and the open circles are MC. There is good agreement.

The charge output (ADC) is given by the time integral of the $V_{\mathrm{PMT}}(t)$ divided by the impedance of the PMT circuit. The width of the simulated

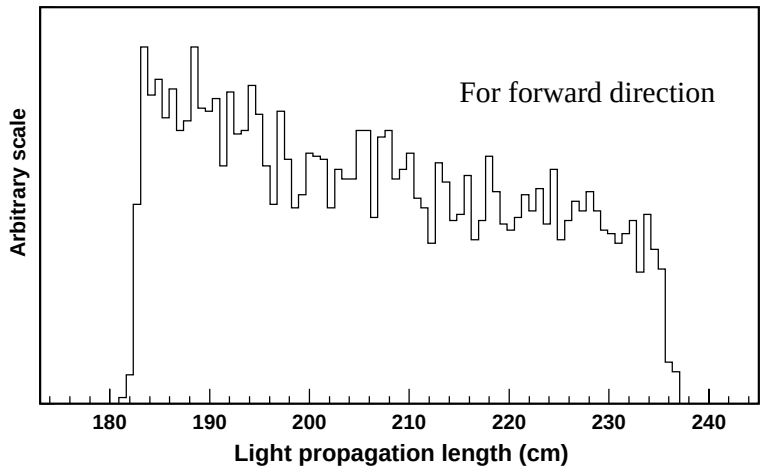

Fig. 8. Light propagation length distribution.

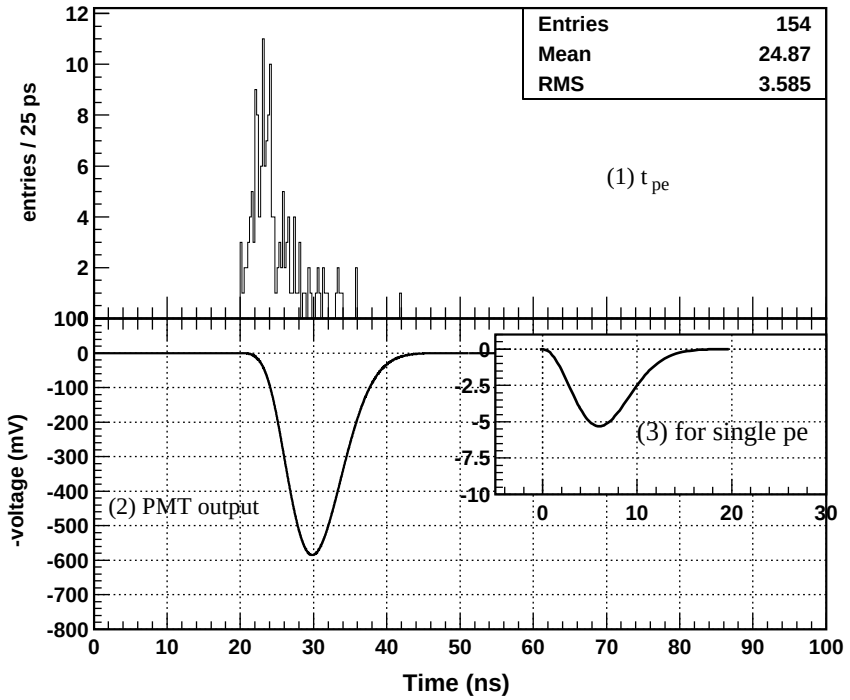

Fig. 9. (1) Time distribution of the photoelectrons, (2) PMT pulse output (with negative sign), and (3) PMT response for a single photoelectron.

charge distribution is narrower than that of the real data. Possible sources of the difference include statistical gain variations of the PMTs [9] (the simulation assumes a constant gain for a single photoelectron), gain variation among individual PMTs, and the imperfection of the simplified model of light propagation. To better represent the data, we adjust the charge distribution by

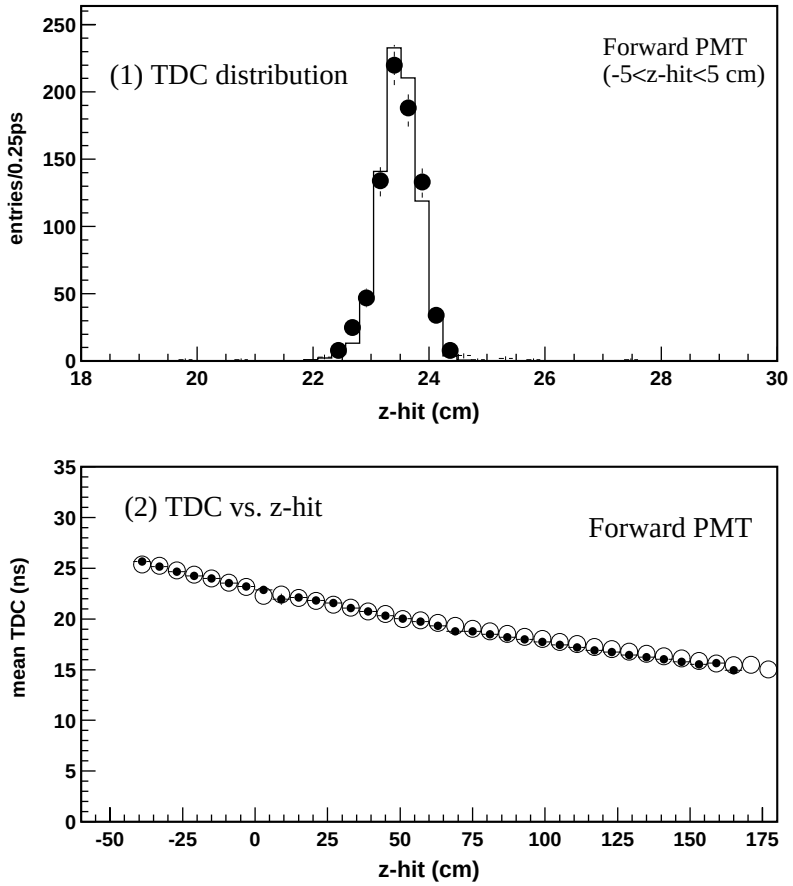

Fig. 10. (1) TDC distribution for $-5 < z\text{-hit} < 5$ cm, (2) TDC distribution as a function of z-hit. The solid circles are data; the histogram and open circles are MC.

introducing a scaled Poisson distribution,

$$\mathrm{ADC} = Q_{\mathrm{orig}}\left(S_{\mathrm{w}}\frac{(N(n_{\mathrm{pe}}) - n_{\mathrm{pe}})}{n_{\mathrm{pe}}} + 1\right) \qquad (10)$$

where ADC is the corrected charge, S_{w} is the width scale parameter, $N(n_{\mathrm{pe}})$ is a random number given by a Poisson distribution generator which has mean n_{pe} and Q_{orig} is the original charge from the $V_{\mathrm{PMT}}(t)$ integration. In a comparison between Q_{orig} and real data, we found that a value $S_{\mathrm{w}} = 2$ gives the best agreement. Fig. 11(1) shows the resulting charge distribution compared with the real data. Fig. 11(2) shows the mean ADC value as a function of the z-hit position. All points are in good agreement. By fitting $\log(\mathrm{ADC}_F/\mathrm{ADC}_B)$ as a function of z-hit (see Fig. 11(3)) to a linear function, we obtain good agreement for the effective light attenuation length (λ) along the z-direction [1].

One of the main parameters in the TOF calibration and reconstruction is a time walk correction coefficient that is used to remove a pulse height dependence [1] of the digitized time. It is the coefficient of a $1/\sqrt{\mathrm{ADC}}$ term, and is sensitive to the rise time of the PMT signal. Fig. 12 shows the (uncorrected) TDC versus $1/\sqrt{\mathrm{ADC}}$ for data and MC. They are in good agreement.

[1] After 30 months of data taking, we observed an attenuation length 13% smaller than the initial value due to aging of the scintillator. The data shown in this figure are from the initial stages of the experiment.

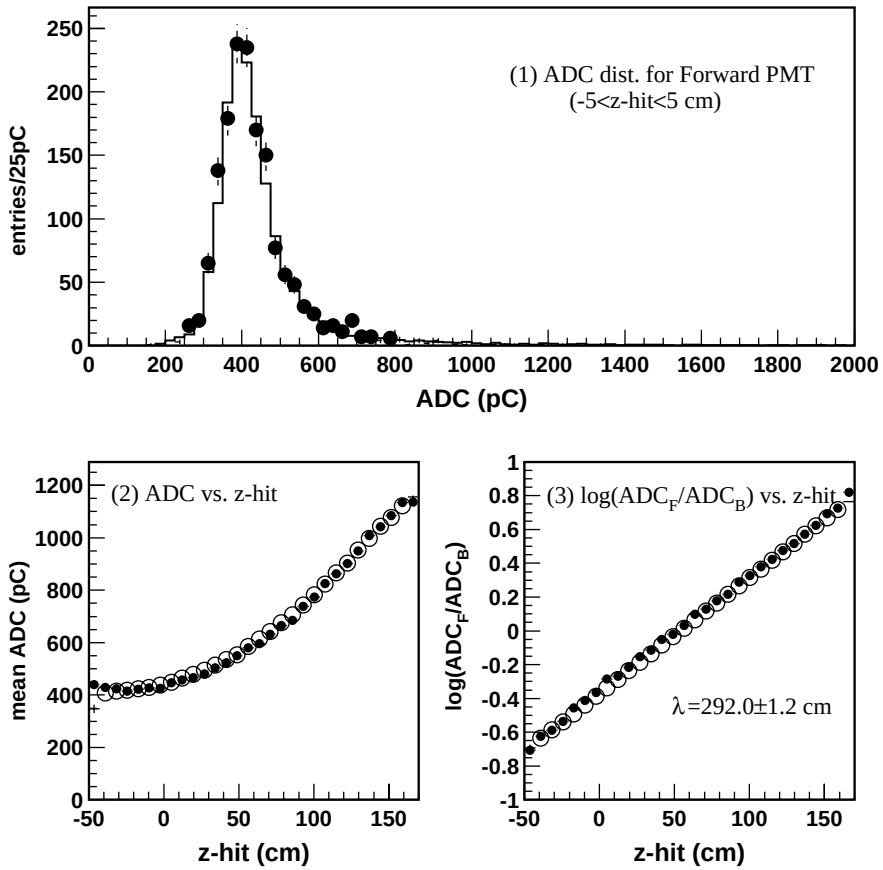

Fig. 11. (1) ADC output distribution. (2) Mean ADC value as a function of z-hit. (3) Dependence of $\log(\mathrm{ADC}_F/\mathrm{ADC}_B)$ on z-hit. The solid circles are data; the histogram and open circles are MC.

3.6. Beam background simulation

The effect of the beam background is simulated by merging beam background data into the MC signal output. The background data are taken by random triggers during the real experiment. The typical hit rate of a single TOF PMT is 15–25 kHz. Because of its greater scintillator width, the TSC counter hit rate is more than 2 times higher than the TOF rate. The hit rates are expected to increase in the higher luminosity environment in the near future.

Fig. 13 presents a flow chart of the beam background merging. For each PMT, MC and background are merged on an event-by-event basis. First, we consider the overlapping of two PMT signals. According to the algorithm in the readout electronics, if two signals are closer than the ADC gate width (100 ns), we take only the earlier signal TDC and the charge of the later signal is added to the earlier one. Otherwise, both signals are recorded. Then the QTC dead time and the number of edges are taken into account.

The major effect of the beam background is to increase the inefficiency caused by the QTC dead time, due to signal conversion and recovery times. It is simulated by discarding the later TDC signal in the case that the MC and beam background times are closer than the QTC dead time, which is found to be 0.55 ns per ADC count (Each ADC count corresponds to a charge of 0.25 pC.) in real data.

Another source of inefficiency is the limit on the number of records in the TDC1877 system [2]. The

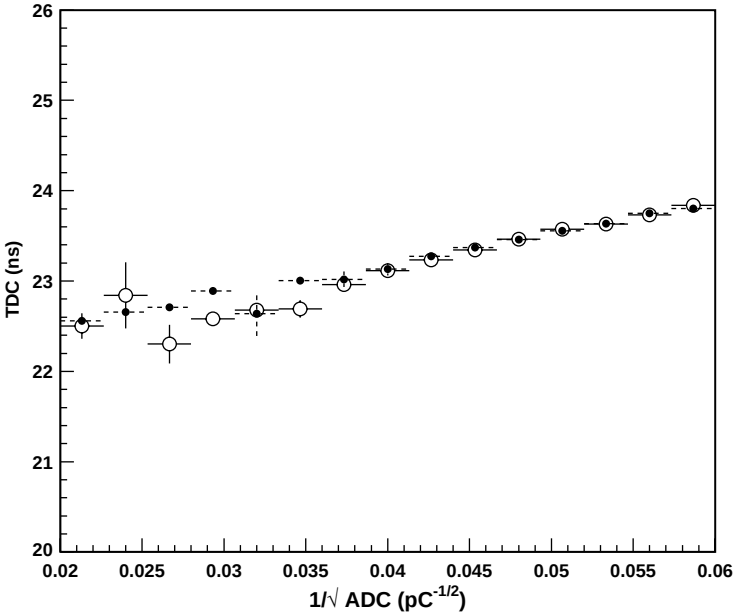

Fig. 12. Variation of the TDC output versus $1/\sqrt{\text{ADC}}$ for $-5<z\text{-hit}<5$ cm. The solid circles are data and the open circles are MC. The TDC and ADC values are for the forward PMTs.

limit is 8 edge records for each PMT in an event. Because the TS system produces 4 edges for one PMT signal [1], a maximum of 2 PMT signals can be recorded for an event. In our simulation, we count the number of edges for the individual TDC channels, and remove the signal(s) after the 8th edge in the merged data. Since we do not use the TS for the TSC counters, this inefficiency is not present for them.

Fig. 14 shows the TOF and TSC hit inefficiencies in μ-pair events ($e^+e^- \to \mu^+\mu^-$) as a function of the TOF trigger rate, which is defined as the rate for at least one TOF-TSC coincidence among the 64 TSC counters. The TOF PMT singles rate is about 25% of this TOF trigger rate, and the TSC singles rate is about two times the TOF singles rate. Here the hit inefficiency is defined as the fraction of muons predicted to hit a TOF counter for which there is no associated counter signal. In the figure, the solid circles are for data and the open circles are for MC with beam background. The hatched part indicates the inefficiency given by the original MC without beam background. This intrinsic inefficiency is due to the dead space between counters. The higher TSC inefficiency is due to the higher background rate. The hit inefficiencies for MC and data agree to within 0.3%.

4. Result

Fig. 15 shows the $dt = T_{\text{obs}}^{\text{correct}} - T_{\text{pred}}$ distribution for all available TOF hits in a μ-pair event sample. Here T_{pred} is the time of flight predicted using the track path length calculated from the fit to hits in the CDC, and $T_{\text{obs}}^{\text{correct}}$ is the weighted average of the observed times in the forward and backward PMTs after correction for the z-hit position and time walk [1]. The distribution is fitted to a symmetric Gaussian to determine the time resolution. The overall time resolution (100 ps) is well represented by the MC. Fig. 16 shows the time resolutions for forward and backward PMTs and for the weighted average time as a function of z-hit .

The PID from the Belle TOF system is based on a ratio of likelihoods for two particle hypotheses.

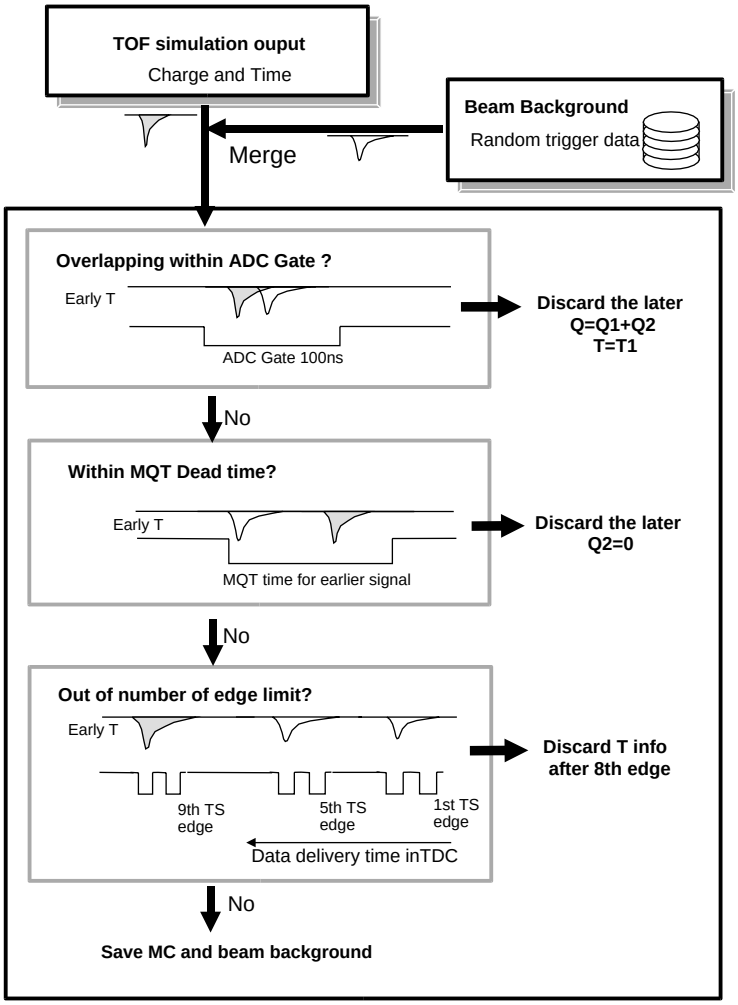

Fig. 13. Flow chart for the merger of beam background with simulated events.

For K/π separation, a particle is identified as a kaon using the likelihood ratio $\mathrm{PID(K)} = P_K/(P_\pi + P_K)$, where the $P_{K,\pi}$ are the PID likelihoods for the particle hypotheses in the subscripts. The PID performance is evaluated using the charm decay $D^{*+} \to D^0\pi^+$, followed by $D^0 \to K^-\pi^+$. Fig. 17 shows the measured K ID efficiency and π fake rate as a function of momentum, where $\mathrm{PID(K)} > 0.6$ is required to identify a kaon. The MC reproduces the K ID efficiency and fake rate as functions of momentum with maximum deviations of 0.7% and 1.8%, respectively.

5. Conclusion

In this report we describe the full detector simulation for the Belle TOF system. We developed a GEANT-based simulator for the processes in the scintillator and the PMT, the readout electronics of the discriminator and the QTC, and the effect of beam background.

Scintillation light is produced using the hit information from GEANT. Using simple models for light propagation in the TOF scintillator and for the PMT response, we accurately reproduce the real PMT signals. The simulation represents

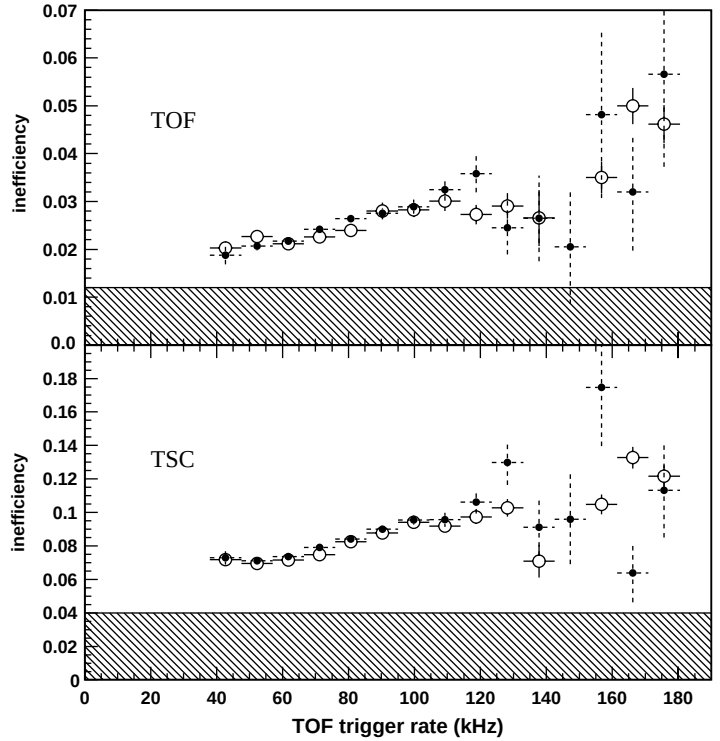

Fig. 14. Hit inefficiency as a function of the TOF rate. The solid circles are data and the open circles are MC.

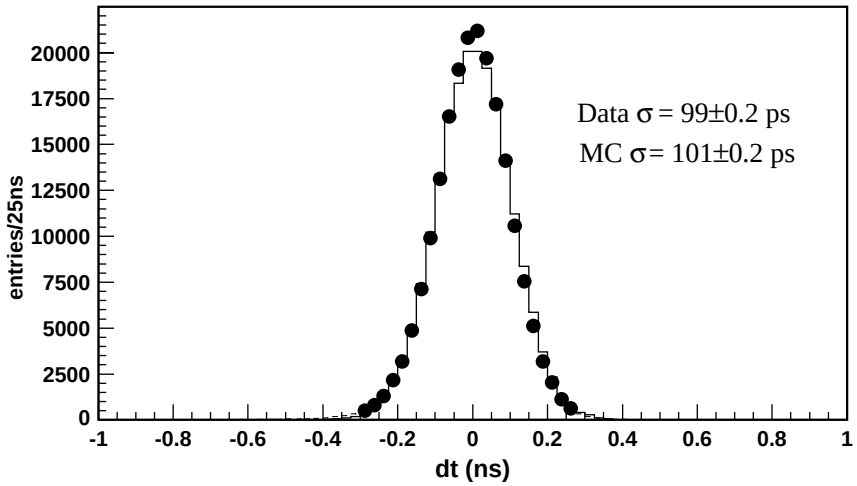

Fig. 15. The dt distribution. The circles are data; the histogram is MC.

the detector characteristics of the TOF system such as light attenuation, the ADC distribution, the effective light velocity, the TDC distributions and the time resolution. Through a beam background merging process, the QTC dead time and the limit on the number of records in the TDC1877 system is simulated, so that the TOF hit inefficiency dependence on the background rate is

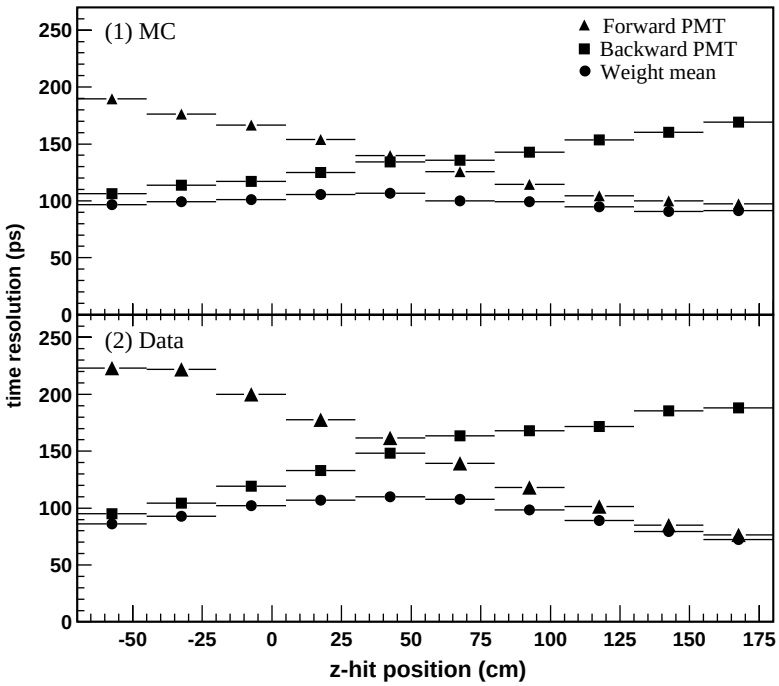

Fig. 16. TOF resolution as a function of z-hit. The top panel is MC; the bottom is data.

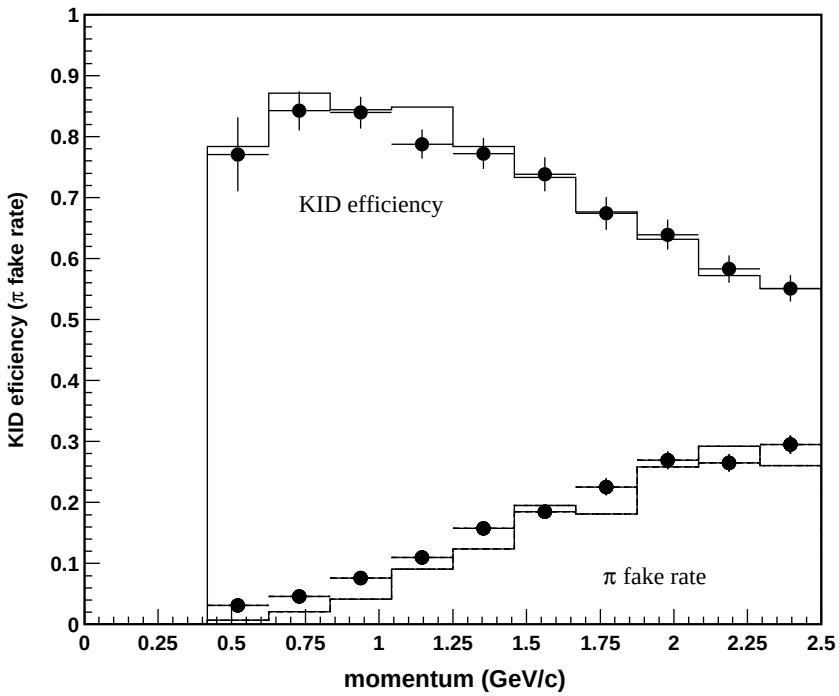

Fig. 17. K ID efficiency and π fake rate as a function of momentum. The circles are data; the histogram is MC.

accurately modeled. Since the dependence on pulse height and on z-hit is well reproduced, the simulation is a good tool for the investigation and development of calibration and reconstruction methods. The K ID efficiency and its momentum dependence are in good agreement with the data. The TOF simulation provides an important component of the Belle MC used for physics analysis.

Acknowledgements

We wish to thank the Belle collaboration and KEKB accelerator group. We acknowledge support from the Ministry of Education, Culture, Sports, Science, and Technology of Japan and the Japan Society for the Promotion of Science; the BK21 program of the Ministry of Education of Korea and the Center for High Energy Physics sponsored by the KOSEF; and the US Department of Energy.

References

[1] H. Kichimi, et al., Nucl. Instr. and Meth. A 453 (2000) 315.
[2] K. Abe et al.,(Belle Collaboration), Nucl. Instr. and Meth. A 479 (2002) 117.
[3] KEKB B Factory Design Report, KEK Report 95-7, 1995, unpublished;
Y. Funakoshi et al., Proceedings of the European Particle Accelerator Conference, Vienna, 2000.
[4] CERN Program Library Long Writeup W5013, CERN, 1993.
[5] H. Kichimi, et al., Nucl. Instr. and Meth. A 325 (1993) 451.
[6] D. Clark, Nucl. Instr. and Meth. 117 (1974) 295.
[7] C.M. Hawkes, et al., Nucl. Instr. and Meth. A 292 (1990) 329.
[8] Photomultiplier Tubes: Basics and Applications, 2nd Edition, Hamamatsu Photonics K.K., 1999.
[9] R. Suda, et al., Nucl. Instr. and Meth. A 406 (1998) 213.